Structures and Polymorph-Sensitive Luminescence Properties of BiPO4/Eu Grown in Hydrothermal Conditions

ARTICLE *in* CRYSTAL GROWTH & DESIGN · JULY 2012

Impact Factor: 4.89 · DOI: 10.1021/cg300451d

5 AUTHORS, INCLUDING:

Minglei Zhao
New York University
23 PUBLICATIONS **391** CITATIONS
SEE PROFILE

Guangshe Li
Chinese Academy of Sciences
178 PUBLICATIONS **4,157** CITATIONS
SEE PROFILE

Liping Li
Chinese Academy of Sciences
205 PUBLICATIONS **4,240** CITATIONS
SEE PROFILE

Liusai Yang
Chinese Academy of Sciences
20 PUBLICATIONS **311** CITATIONS
SEE PROFILE

CRYSTAL GROWTH & DESIGN

Article

pubs.acs.org/crystal

Structures and Polymorph-Sensitive Luminescence Properties of $BiPO_4$/Eu Grown in Hydrothermal Conditions

Minglei Zhao,[†] Guangshe Li,[‡] Liping Li,*[,†] Liusai Yang,[†] and Jing Zheng[†]

[†]Key Lab of Optoelectronic Materials Chemistry and Physics, Fujian Institute of Research on the Structure of Matter, Graduate School of Chinese Academy of Sciences, Fuzhou 350002, P. R. China

[‡]State Key Lab of Structural Chemistry, Fujian Institute of Research on the Structure of Matter, Chinese Academy of Sciences, Fuzhou 350002, P. R. China

Supporting Information

ABSTRACT: In this work, $BiPO_4$/Eu of different polymorphs was prepared using a simple hydrothermal method. It is found that a hexagonal phase (HP) was formed at 100 °C, which transformed to a low-temperature monoclinic phase (LTMP) when hydrothermal temperature was increased to 160 °C. This LTMP transformed reversely to HP when the temperature increased beyond 180 °C. This phase evolution is quite distinct from those when using high-temperature calcinations (*CrystEngComm*, 2011, *13*, 6251−6257). Accompanying this phase evolution, sample morphology varied from homogeneous rodlike shape to prismlike shape, while the lattice strain features changed from tensile to compressive, and then to tensile, as followed by a decrease in symmetry of tetragonal PO_4 groups from pseudo-T_d to C_1. These variations were closely related to the reaction mechanism in solution chemistry, in which two interfacial processes were indicated, differing from the ionic diffusion process during calcination. As a consequence, luminescence properties become sensitive to polymorphs. All Judd−Ofelt parameters (Ω_λ, λ = 2, 4, 6) were calculated to evaluate the asymmetric nature for the polymorph-sensitive luminescence. It is found that the Ω_2 value for HP was 1.66×10^{-20} cm^2, which increased to 2.10×10^{-20} cm^2 for LTMP; meanwhile, the quantum efficiency increased from 9.33% for HP to 36.09% for LTMP. These results demonstrated that $BiPO_4$ of different polymorphs can be obtained through the hydrothermal method, which may enrich the significance of solution chemistry in preparing advanced materials of tailored functionalities.

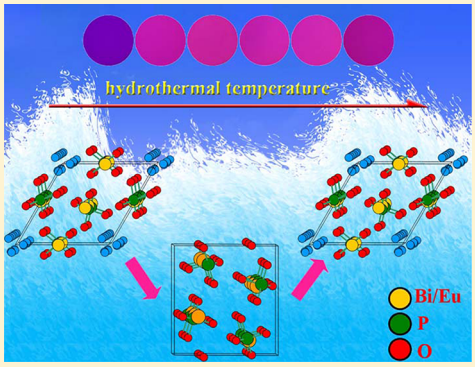

1. INTRODUCTION

Hydrothermal synthesis has been proved successful for preparing novel materials (e.g., microporous crystals, superionic conductors, gel-inspired materials, nanometer particles, and particularly stacking-sequence materials).[1−5] Besides the preparation of new materials, hydrothermal synthesis has been important in simulating biological and environmental processes which give some understanding of the origin of life and the supercritical water oxidation process for decomposing organic wastes.[6,7] As one of the most effective routes, hydrothermal synthesis has also been taken to stabilize some metastable polymorphs that usually cannot be obtained through traditional solid-state reactions.[8−10] For instance, *t*-$LaVO_4$, a metastable phased material, can only be prepared by a solution process.[11] Till now, acquirement and stabilization of metastable phases with desirable properties are currently among the most challenging objectives in inorganic chemistry, material sciences, and many other disciplines.[12,13] In spite of some great progresses, exploration of hydrothermal synthesis of polymorphs is still a hot subject,[14,15] since some metastable polymorphs can be thus prepared to show novel properties essential for many relevant technological applications.

It is documented that metastable phases can readily transform to the thermodynamically stable phases by conventional methods such as high-temperature calcinations, while the reverse process is rather difficult, and even impossible, without involving any chelating ligands or additives.[16−18] One may anticipate that if phase structures of inorganic compounds can be continuously adjusted by hydrothermal conditions, transforming from the metastable phases to the thermodynamically stable phases, and reversely to the metastable phase, then many attractive properties would be highly possible.

Here, we choose Eu^{3+} doped $BiPO_4$ as a model compound to study, based on the following considerations: (i) $BiPO_4$ has several polymorphs, in which the hexagonal phase (HP) is metastable and can be prepared at room temperature;[19] (ii) Eu^{3+} can be doped in $BiPO_4$ at ambient conditions because of an ionic size closer to that of Bi^{3+};[20] and more importantly, (iii) upon doping, Eu^{3+} could be taken as an effective probe to investigate the local structures and polymorph-sensitive luminescence properties that follow the phase evolutions

Received: April 3, 2012
Revised: July 2, 2012
Published: July 10, 2012

under hydrothermal conditions. In this work, we used a facile hydrothermal method to prepare $BiPO_4$ of different polymorphs. It is demonstrated that the phase evolutions and luminescence performance of the as-prepared samples were quite different from those obtained by high-temperature calcinations. The results reported in this work may pave an alternative way to tailor the luminescence properties for many applications through systematic control over the polymorphs.

2. EXPERIMENTAL SECTION

2.1. Sample Preparation. All chemicals of analytical grade were used without further purification. In a typical experiment, 5 mL of an ethylene glycol solution of $Bi(NO_3)_3{\cdot}5H_2O$ (1.9 mmol), 0.1 mmol $Eu(NO_3)_3{\cdot}6H_2O$, and 2 mmol $NH_4H_2PO_4$ was dissolved in 65 mL of deionized water under constant stirring for 30 min. A homogeneous white suspension was formed, which was transferred into a Teflon-lined stainless-steel autoclave. The autoclave was tightly closed and maintained at the given temperature for 12 h, and it was naturally cooled down to room temperature. Finally, white precipitates were synthesized, collected, washed with distilled water several times, and dried at 60 °C for 6 h for further characterization.

2.2. Sample Characterization. Powder X-ray diffraction (XRD) patterns of the samples were collected using a Rigaku Miniflex apparatus equipped with Cu Kα radiation (λ = 0.15418 nm). Phase compositions and lattice parameters were calculated using a profile fitting by a least-squares method employing the computer GSAS program[21] implemented with EXPGUI, in which Ni powders served as an internal standard for peak positions calibration (as illustrated in Figure S1 of the Supporting Information). FT-IR spectra of the samples were recorded on a Perkin-Elmer Spectrum One spectrometer in the range 400−4000 cm^{-1} with the resolution of 4 cm^{-1} using KBr as a diluting agent. The mass ratio of the samples to KBr is set to the given values, i.e. 6‰, 5‰, 6‰, and 7‰ for the samples obtained at 100, 140, 180, and 240 °C, respectively. Raman spectra of the samples were obtained on a Renishaw Raman microscope InVia Plus system with an excitation line of 785 nm. Field-emission scanning electron microscopic (FE-SEM) images of the samples were taken by a JEOL JSM-6700 operated at 10.0 kV beam energy.

2.3. Luminescence Measurements. Photoluminescent spectra of the samples were carried out at room temperature by a Varian Cary Eclipse Fluorescence Spectrometer. In order to fully evaluate the luminescence performance of the samples, excitation spectra were measured in the range of 200−550 nm, and the emission spectra were recorded in the range of 400−850 nm. Decay time curves were recorded by single photo counting with a Cary Eclipse Lifetimes Application setup.

3. RESULTS AND DISCUSSION

3.1. Polymorphic Controls. Figure 1 shows the XRD patterns of the samples. When the reaction temperature of the hydrothermal system was as low as 100 °C, all diffraction peaks matched well a hexagonal phase (HP, JCPDS, card no. 45-1370), while no other peaks from Eu_2O_3 or impurities can be detected, which indicates a pure HP phase. As the temperature increased to 120 °C, the LTMP component appeared, as characterized by very weak diffraction peaks (011) and (−111) around 19.4° and 21.8°, respectively. LTMP became the dominant phase when the reaction temperature further increased. For instance, when the temperature increased up to 140 °C, the content of the LTMP component was about 81.4 wt %, as illustrated in Table 1.

When the hydrothermal temperature was raised to 160 °C, all diffraction peaks could be readily indexed to a low-temperature monoclinic phase (LTMP, JCPDS, No. 15-0767), which remained as the hydrothermal temperature increased to 180 °C. Upon further increasing the temperature to 200 °C, the

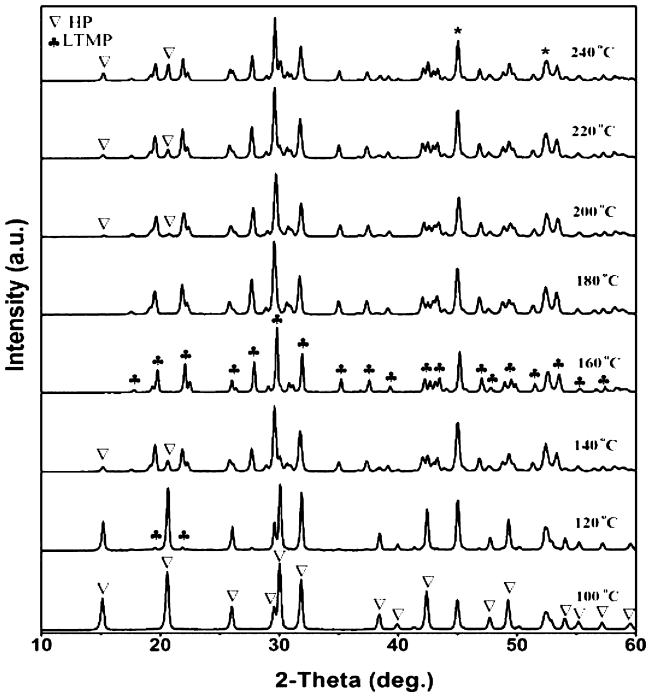

Figure 1. XRD patterns of the samples prepared in hydrothermal conditions at given temperatures for 12 h. Symbol * represents the diffraction lines of the internal standard, nickel.

HP phase reappeared, as indicated by the presence of weak diffraction peaks (100) and (101) around 15.2° and 20.7°, respectively. The phase composition of HP increased with the hydrothermal temperature. For instance, the content for the HP component was 3.9 wt % at 200 °C, which increased up to 25.4 wt % at 240 °C. All these demonstrate that the polymorphs of $BiPO_4$/Eu can be readily tuned by adjusting the reaction temperature of hydrothermal systems.

It is noted that the phase evolutions under hydrothermal conditions are quite different from those upon high-temperature calcinations. For the present system, HP transformed into LTMP at 140 °C, a temperature much lower than that of 500 °C when using high-temperature calcinations.[19] Further, an abnormal phase transformation from LTMP to HP occurred in the present hydrothermal system, as reaction temperature is beyond 180 °C, which is difficult to understand by the thermodynamic process. Generally speaking, higher temperatures are usually beneficial for forming the thermodynamically stable phases, as confirmed by our recent work, in which phase transformation from LTMP to HTMP was observed at temperatures >600 °C using high-temperature calcinations.[22] In order to confirm this phase transformation process, another set of samples was prepared under the given reaction conditions. As indicated in Figure S2 by the comparative XRD patterns, the phases/phase mixtures in the transformation are well reproducible in hydrothermal conditions. Especially, HP appeared again as the reaction temperature increased above 180 °C. The presence of HP at higher temperatures for the present systems might be associated with the unique characteristics of hydrothermal conditions, *i.e.* high pressure, and subcritical state, which will be further investigated.

Accompanying the phase transformation is the variation in lattice symmetry: HP has a structural symmetry much higher than that for LTMP, and therefore, transformation from HP to LTMP is thermodynamically favorable. For such a trans-

dx.doi.org/10.1021/cg300451d | *Cryst. Growth Des.* 2012, 12, 3983−3991

Table 1. Phase Fraction and Lattice Parameters of $BiPO_4$/Eu Prepared at Different Hydrothermal Temperatures

			cell parameters (Å)							
	phase fraction (%)		HP phase			LTMP phase				
temp (°C)	HP	LTMP	a (Å)	c (Å)	V (Å^3)	a (Å)	b (Å)	c (Å)	β	V (Å^3)
100	100	0	6.9684(1)	6.4605(2)	271.68(1)					
120	90.0	10.0	6.9929(2)	6.4833(2)	274.56(2)	6.737(1)	6.927(2)	6.459(1)	103.70(2)	292.86(8)
140	18.6	81.4	6.9831(6)	6.4749(9)	273.44(5)	6.7541(3)	6.9437(3)	6.4751(3)	103.736(4)	294.99(2)
160	0	100				6.7532(2)	6.9445(2)	6.4732(2)	103.728(3)	294.91(2)
180	0	100				6.7551(3)	6.9461(3)	6.4755(3)	103.718(4)	295.18(3)
200	3.9	96.1	6.956(2)	6.453(4)	270.4(2)	6.7543(2)	6.9441(2)	6.4743(2)	103.718(3)	295.00(1)
220	11.4	88.6	6.990(1)	6.472(2)	273.87(7)	6.7523(2)	6.9434(2)	6.4725(2)	103.710(3)	294.81(1)
240	25.4	74.5	6.9768(4)	6.4618(6)	272.40(3)	6.7543(3)	6.9426(3)	6.4751(3)	103.703(4)	294.99(3)

formation process, the temperature effect might be a dominant factor. Namely, the content of the LTMP component increased gradually with the reaction temperature, until a pure LTMP phase was formed, as indicated by the XRD analysis in Figure 1. With regard to the transformation from a low-symmetry phase to a high-symmetry one, one may have to consider several factors, such as reaction pressure, impurities, and/or some absorbent molecules (e.g., water).[23] Generally, the above transformation usually requires a much higher pressure (e.g., >10^9 Pa),[18,24] which appears very difficult to reach for a common hydrothermal system. For instance, with the hydrothermal reactor shown in Figure S3 of the Supporting Information, the pressure was determined to be 3.2 bar (i.e., 3.2 × 10^5 Pa) at 100 °C, which increased to 8.5 bar (i.e., 8.5 × 10^5 Pa) at 180 °C, and to 15.2 bar (i.e., 1.52 × 10^6 Pa) at 220 °C. As this point, the reaction pressure could not be a dominant factor responsible for the abnormal transformation from stable LTMP to metastable HP. Further, no signals of impurities were detected from XRD patterns and the following luminescence data, which excludes the impurities from a possible reason. Based on these considerations, the above transformation might be associated with the reaction medium of water, which could enter the lattice structure and bring about the changes in polymorphs or forming certain hydrated phases. After all, the high-symmetry phase HP was indeed a hydrated phase.

Variations in morphologies and particle sizes that accompany the polymorphic changes of $BiPO_4$ were examined. As indicated by the SEM images in Figure 2a, HP obtained at room temperature consisted almost entirely of nanorods with diameters of 20−80 nm and lengths ranging from several nanometers to hundreds of nanometers. When the reaction temperature was set at 100 °C, either phase structure or rodlike morphology was maintained, except for the particle sizes: the bigger particles grew up at the expense of the shrinkage of the smaller particles, characteristic of an Ostwald ripping process (Figure 2b). With increasing the hydrothermal reaction temperature, phase transformation from HP to LTMP occurred, resulting in the variation of morphology from nanorods to much bigger prism-shaped particles. For instance, when prepared at 140 °C, the products were composed of a mixture of nanorods and prism-shaped particles (Figure 2c). Increasing the temperature up to 180 °C led to the pure LTMP phase with a morphology that is composed of nearly all prism-shaped particles (Figure 2d). Upon further increasing the hydrothermal temperature to 240 °C, the HP phase reappeared, as indicated by the presence of some small nanorods again in Figure 2e. These observations were quite different from our previous report by high-temperature calcinations,[19] where the

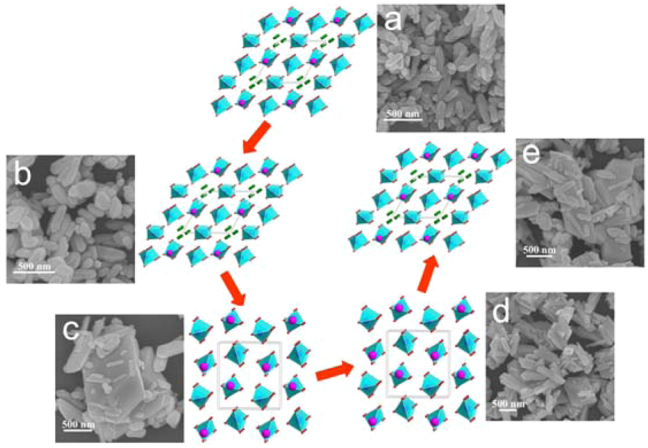

Figure 2. Morphological evolutions with phase structure transformation for the samples obtained at given temperatures: (a) room temperature, (b) 100 °C, (c) 140 °C, (d) 180 °C, and (e) 240 °C.

morphology changed from homogeneous nanorods to a nearly spherical-like shape with phase evolution from HP to LTMP.

3.2. Microstructure Changes with Polymorphs. Microstructure changes with polymorphs were investigated by FT-IR spectra. As shown in Figure 3, the main absorption band in the region of hydroxyl stretching is centered at 3496 cm^{-1}. According to the literature, this band can be assigned to the stretching vibration, ν(O−H), of the water coordinated directly

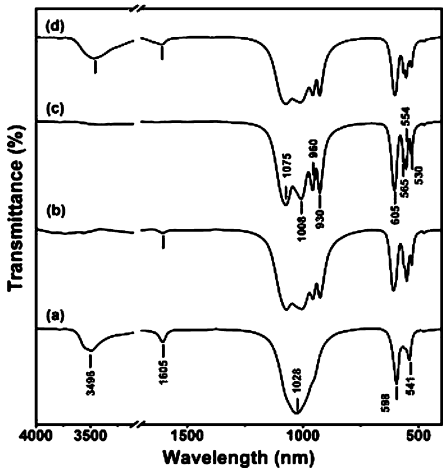

Figure 3. FT-IR spectra of the samples prepared in hydrothermal conditions at given temperatures: (a) 100 °C, (b) 140 °C, (c) 180 °C, and (d) 240 °C.

dx.doi.org/10.1021/cg300451d | Cryst. Growth Des. 2012, 12, 3983−3991

to the bismuth atoms in the HP phase.[25,26] It should be mentioned here that lattice hydrogen in the form of O−H can be very difficult to be excluded, though hydrogen atoms are always easy to be incorporated in the samples during solution growth to play a similar role to that of the lattice water.[5] Another band associated with hydroxyls is located at 1605 cm^{-1}, which characterizes the vibrations δ(H−O−H). Both stretching and bending vibrations for O−H groups become gradually weak in intensity with increasing the hydrothermal temperature, and they nearly disappear around 180 °C. Further increasing the temperature, the vibrations for O−H groups become gradually strong again. These variations were consistent with the above structural evolutions.

Symmetric changes of PO_4 tetrahedra with polymorphs were also investigated by FT-IR. As shown in Figure 3, some distinct differences can be clearly seen in their vibrational characteristics with respect to phosphate groups. Based on group-theoretical analysis,[27] the isolated PO_4 group has T_d symmetry with nine internal modes that can be presented as

$$\Gamma_{vib} = A_1 + E + 2F_2 \quad (1)$$

where the E representation is doubly degenerated and F_2 is triply degenerated. The mode belonging to the A_1 representation and one of the triply degenerated F_2 modes correspond to the symmetric (ν_1) and asymmetric (ν_3) P−O stretching vibrations of the PO_4 group, respectively, whereas the other F_2 mode and the E mode representation correspond to O−P−O bending ν_2 and ν_4, respectively. For isolated PO_4 tetrahedra in aqueous solution, the experimental wavenumber values for ν_1, ν_2, ν_3, and ν_4 are 938, 420, 1017, and 567 cm^{-1}, respectively.[28] Once the phosphate groups are incorporated into the crystal lattice, depending upon the symmetry around the phosphate group and the nature of the charge balance cation, the above modes undergo either blue shift or red shift. For the present work, PO_4 groups in HP obtained at 100 °C have a C_2 symmetry with two different P−O bond lengths (1.433 and 1.590 Å, Table S1), and it can be considered to have a pseudo-T_d symmetry (Figure 3a). Under this symmetry, the ν_1 and ν_3 modes of vibration are so close that they overlap significantly to give a very intense band centered at 1028 cm^{-1}. The corresponding ν_2 and ν_4 modes appeared around 598 and 541 cm^{-1}, respectively.[29] With increasing the hydrothermal temperature, the ν_3 stretching vibration of the PO_4 group was gradually split, characteristic of LTMP. For instance, the symmetry of the PO_4 groups in LTMP prepared at 180 °C is further lowered to C_1 (Figure 3c), since all four P−O bonds are different, with lengths varying between 1.344 and 1.672 Å. Based on the previous studies on different phosphates,[30−33] bands at 1075, 1008, and 960 cm^{-1} have been assigned to the ν_3 asymmetric stretching vibration of P−O bonds and that around 930 cm^{-1} is attributed to the corresponding ν_1 symmetric vibration. The bending vibration of O−P−O linkages appeared around 605, 565, 554, and 530 cm^{-1}.

The symmetry changes of PO_4 tetrahedra with polymorphs were further examined by Raman. As shown in Figure 4, for the samples obtained at 100 and 240 °C, the majority of the Raman bands were broadened, likely due to the presence of lattice water molecules in HP. The Raman spectrum for LTMP obtained at 180 °C contains relatively narrow bands which are clearly distinguishable from HP. In all four spectra, the observed intense band at 170 cm^{-1} and a shoulder at 231 cm^{-1} are due to the Bi−O stretching vibration.[34] The bands centered at 1038 and 970 cm^{-1} are ascribed to the asymmetric

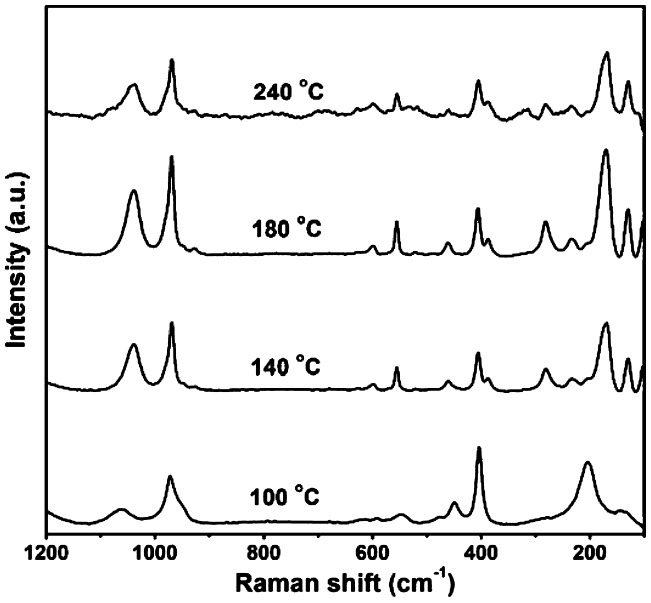

Figure 4. Raman spectra of the samples prepared in hydrothermal conditions at given temperatures for 12 h.

(ν_3) and symmetric (ν_1) stretching vibrations of the PO_4 group, respectively. The bands in the region between 550 and 600 cm^{-1} correspond to the ν_4 bending vibration modes of PO_4 groups. The weak bands at 406 and 460 cm^{-1} can be assigned to the ν_2 bending vibration of the PO_4 unit.[35] It is noted that the broadening effects of lattice water in HP make it very difficult to see any apprent differences in the Raman spectra, though the structure symmetry of PO_4 tetrahedra for polymorphs is different, as reflected by FT-IR spectra.

Lattice variations with polymorphs were further examined by evaluating the lattice parameters. As listed in Table 1, as the reaction temperature increased from 100 to 140 °C, the lattice parameter, a, of HP first increased and then decreased. When the reaction temperature further increased from 200 to 240 °C, the lattice parameter, a, of HP still increased and then decreased. Meanwhile, the variation of c follows a similar trend. For the LTMP phase, abnormal variation of lattice parameters was also observed in the phase transformation process. For instance, a increased first, and then decreased, when the content of LTMP increased. Afterward, a decreased and then increased. It was well-known that the lattice parameters could be influenced by many factors, such as size effect, valence-state and/or spin-state transitions, doping level, and interfacial process, as those occurred during phase transformations.[36] In this regard, size effect was first excluded, since the diameters for the majority of particles were beyond 100 nm. Second, no valence-state or spin-state transitions were observed in the present samples. Third, the doping ions and doping levels were kept almost the same for all samples. Instead, for the present case, the above abnormal variations of lattice parameters were probably associated with the interfacial process during the phase transformation. All these changes would show an impact on the luminescence properties as described below.

Strain changes with polymorphs were calculated by broadening effects of diffraction peaks using the Williams and Hall theorem,[36,37]

$$\frac{\beta \cos\theta}{\lambda} = \frac{1}{D} + \frac{\eta \sin\theta}{\lambda} \quad (2)$$

dx.doi.org/10.1021/cg300451d | Cryst. Growth Des. 2012, 12, 3983−3991

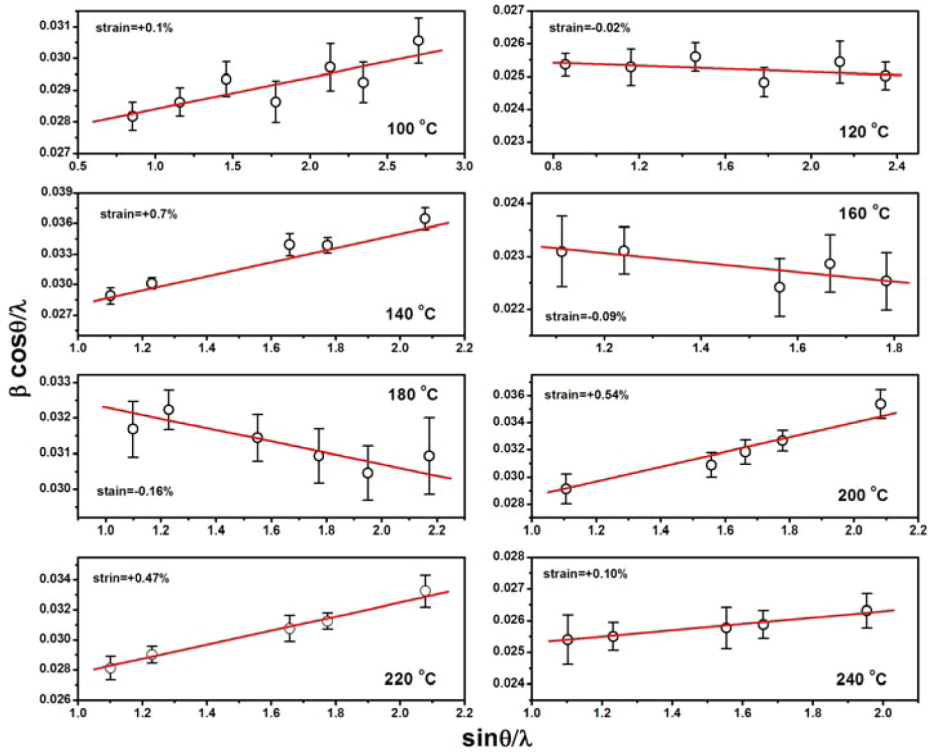

Figure 5. Relationship between $(\beta \cos\theta)/\lambda$ and $(\sin\theta)/\lambda$ for the samples prepared in hydrothermal conditions at given temperatures for 12 h.

where β is the full width at half-maximum (fwhm), θ is the diffraction angle, λ is the X-ray wavelength, D is the effective particle size, and η is the effective strain. The strain is determined from the slope of a plot of $\beta \cos\theta/\lambda$ vs $\sin\theta/\lambda$. For the sample prepared at 100 °C, the strain was determined to be tensile at +0.1%, which decreased to near zero (−0.02%) as hydrothermal temperature increased to 120 °C (Figure 5), though the HP phase remained unchanged. When the hydrothermal temperature increased to 140 °C, a phase mixture of LTMP and HP was obtained, as dominated by LTMP amounting to 81.4 wt %. The strain for the main phase (LTMP) was tensile at +0.7%. Strikingly, the nature of the strain changed from the tensile to compressive. For instance, when treated at 160 °C, the strain of LTMP was compressive at −0.09%, which was increased to a similar magnitude (−0.16%) as the hydrothermal temperature increased to 180 °C (Figure 5). This compressive strain became tensile again, when HP appeared. The strain for LTMP was tensile at +0.54% when hydrothermal temperature increased up to 200 °C. The strain was then found to decrease to +0.47% and +0.10% when hydrothermal temperature further increased to 220 and 240 °C, respectively (Figure 5). Although the features of the strain for some samples are difficult to determine in the framework of the error margin, there is indeed a phase/strain dependence given the strain of all samples. These results indicate that the lattice strain could be tuned from tensile to compressive and further from the compressive to tensile by varying the polymorphs. These observations were quite different from the strain behaviors when using high-temperature calcinations.[19]

3.3. Luminescence Changes with Polymorphs. Figure 6 shows the photoluminescent excitation (PLE) spectra of the samples prepared at 100 and 180 °C for 12 h, respectively. The PLE spectra were measured by monitoring the emission $^5D_0$−$^7F_1$ (593 nm) at room temperature in the range of 200−550 nm. It is shown that there exists a broad intense band at

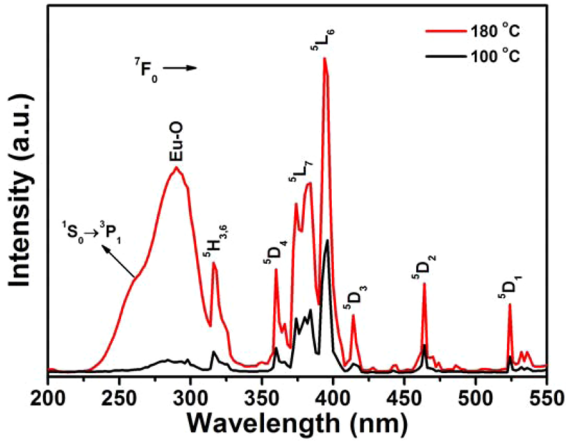

Figure 6. Typical excitation spectra of 5 mol % Eu^{3+}-doped $BiPO_4$ prepared in hydrothermal conditions at 100 and 180 °C for 12 h, respectively.

290 nm with a shoulder at around 260 nm, along with many sharp peaks in the wavelength range of 310−550 nm. The broad band centered at 290 nm corresponds to the Eu−O charge-transfer band (CTB), which arose from the transition of the 2p electrons of O^{2-} to the empty 4f orbitals of Eu ions.[38] The shoulder at 260 nm, overlapped to the intense band, is due to the $^1S_0 \rightarrow {}^3P_1$ transition of Bi^{3+} ions.[39,40] Several sharp lines were observed in the longer wavelength region, located at 317, 361, 383, 394, 416, 465, and 525 nm, which correspond to the intrinsic transitions from the ground state, $^7F_0$, to the excitation multiplets, $^5H_{3,6}$, $^5D_4$, $^5L_7$, $^5L_6$, $^5D_3$, $^5D_2$, and $^5D_1$ of Eu ions, respectively.[41] It is also observed that the PLE intensity of both CTB and Eu ions increased with phase transformation from HP (100 °C) to LTMP (180 °C), which infers that LTMP has a

dx.doi.org/10.1021/cg300451d | Cryst. Growth Des. 2012, 12, 3983−3991

higher energy transfer efficiency when compared to HP (Figure 6).

Figure 7 shows the photoluminescent (PL) spectra of the samples obtained at given temperatures for 12 h. The emission

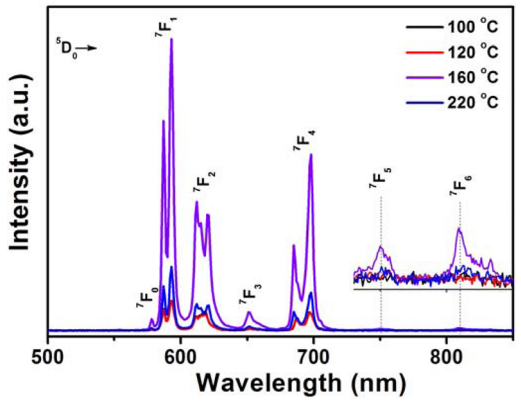

Figure 7. Photoluminescent (PL) spectra of 5 mol % Eu^{3+}-doped $BiPO_4$ in hydrothermal conditions at given temperatures.

spectra were measured at room temperature in the range of 400−850 nm. Upon excitation into the $^7F_0$−$^5L_6$ transition at 394 nm, an orange-red color was observed, characteristic of the transitions $^5D_0$−^7F_J (J = 0, 1, 2, 3, 4, 5, 6) of Eu^{3+} ions. The strong emission bands around 593 and 618 nm are associated with the transitions $^5D_0$−$^7F_1$ and $^5D_0$−$^7F_2$, respectively, while bands in the range of 641−670 and 678−717 nm are assigned to the transitions $^5D_0$−$^7F_3$ and $^5D_0$−$^7F_4$, respectively.[42,43] The weak emssion bands centered at 751 and 810 nm are associated with the transitions $^5D_0$−$^7F_5$ and $^5D_0$−$^7F_6$, respectively.

To get insight into the possible structural changes surrounding Eu^{3+} between two phases, the experimental intensity parameters Ω_2, Ω_4, and Ω_6 were calculated from the emission spectra using a technique developed by Porcher and others.[44,45] This technique takes advantage of the fact that the intensities of the transitions $^5D_0$−$^7F_2$, $^5D_0$−$^7F_4$, and $^5D_0$−$^7F_6$ are mainly dependent on the parameters Ω_2, Ω_4, and Ω_6, respectively. Also, the transition $^5D_0$−$^7F_1$ possesses a magnetic dipole character, whereas other transitions $^5D_0$−^7F_J (J = 2, 4, 6) are characteristic of the electric dipole transitions. It is possible to express the spontaneous emission intensity for an i−k transition as[46]

$$I(i, k) = \hbar\omega_{ik} A(i, k)\, N(i) \tag{3}$$

where $\hbar\omega_{ik}$ is the transition energy and $N(i)$ is the population of the emission probability for the i−k transition.[45] In the case of the emission transition $^5D_0$−^7F_J of Eu^{3+}, the term $A(^5D_0, {}^7F_J)$ can be determined from the equation[47,48]

$$A(^5D_0, {}^7F_J) = \frac{4e^2\omega^3}{3\hbar c^3}\chi \sum_{\lambda} \Omega_\lambda \langle {}^7F_J \| U^{(\lambda)} \| {}^5D_0 \rangle^2 \tag{4}$$

where ω is the angular frequency of the transition, A_{0J} is the coefficient of spontaneous emission, e is the electric charge, c is the velocity of light, h is Planck's constant, and χ is the Lorentz local field correction term that is given by $\chi = \eta(\eta^2 + 2)^2/9$, with refractive index η. Unfortunately, there is little information on the refractive index of $BiPO_4$ at present. Considering the quite similar crystal structure between $BiPO_4$ and $LaPO_4$, it could be reasonable to assume that the refractive index of $BiPO_4$ equals that of $LaPO_4$. Namely, it is 1.36 for HP and 1.39 for LTMP.[49] The terms $\langle {}^7F_J \| U^{(\lambda)} \| {}^5D_0 \rangle^2$ are the squared reduced matrix elements, whose values are independent of the chemical environment of the target ions. The squared reduced matrix elements used here are taken from ref 50, in which the values are 0.0032, 0.0023, and 0.0002 for J = 2, J = 4, and J = 6, respectively. The calculated values of the Judd−Ofelt parameters for HP and LTMP are given in Table 2. The Ω_λ parameters of Eu^{3+} for LTMP are noticeably higher than those for HP. This behavior could be due to the fact that the average crystal filed experienced by lanthanide ions in LTMP is different from that for HP, as reported by others.[45] In particular, the larger Ω_2 for LTMP further indicates that Eu^{3+} probably resides at a more asymmetric environment in LTMP relative to HP. All these may explain why the luminescence intensity of LTMP is much stronger than that of HP.

Table 2. Ω_λ, Judd−Ofelt Parameters for the Different Phases Obtained in Hydrothermal Conditions

sample	Ω_2 (10^{-20} cm^2)	Ω_4 (10^{-20} cm^2)	Ω_6 (10^{-20} cm^2)
HP (100 °C)	1.66	3.64	2.91
LTMP (180 °C)	2.10	4.09	4.06

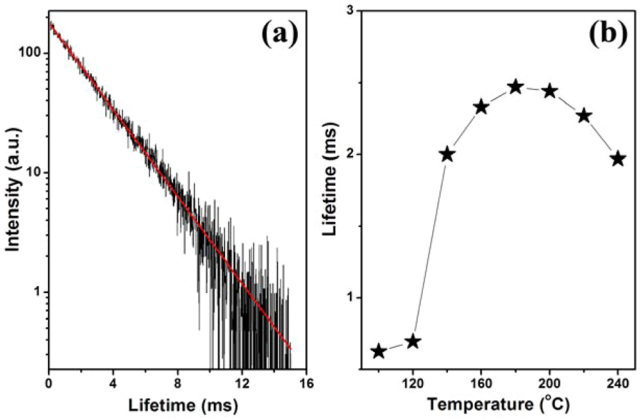

Figure 8. (a) Decay curve for the sample obtained at 180 °C; (b) lifetimes plotted as a function of hydrothermal temperature.

Figure 8a shows the decay curve of the luminescence of Eu^{3+} (593 nm, $^5D_0$−$^7F_1$) in LTMP. The decay curve can be well fitted in a single exponential function,

$$I = I_0 \exp(-t/\tau) \tag{5}$$

where τ is the decay time. The decay time is calculated to be τ = 2.47 ms. Similar decay kinetic behaviors were also observed in other $BiPO_4$ polymorphs. The relationship between decay time and hydrothermal temperature was plotted in Figure 8b. It is seen from Figure 8b that there is no remarkable change in decay time when hydrothermal temperature increase up to 120 °C. However, when HP transformed to LTMP at 140 °C, there appeared a significant change in the decay time, almost 2 times longer than that when reacted at 120 °C. The decay time reached a maximum for the pure LTMP prepared at 180 °C. Further, appearance of HP led to a decrease in the decay time. For instance, the decay time decreased to 2.27 and 1.97 ms when hydrothermally reacted at 220 and 240 °C, respectively. These observations clearly demonstrate that the decay time is

dx.doi.org/10.1021/cg300451d | Cryst. Growth Des. 2012, 12, 3983−3991

also sensitive to the evolution of the polymorphs of $BiPO_4$, which will be further explained in the following discussion.

On the basis of the emission spectra and lifetimes of the $^5D_0$ emitting level, the luminescence quantum efficiency (η) of the Eu^{3+} excited state for different polymorphs can be calculated in terms of the following equation,[51−53]

$$\eta = A_{rad}/(A_{rad} + A_{nrad}) \quad (6)$$

where both terms A_{rad} and A_{nrad} denote the radiative and nonradiative rates, respectively. The terms can be obtained using an integrated region and are defined as[51]

$$A_{rad} = \sum_{J=0}^{6} A_{0J} \quad (7)$$

where $A_{0J} = (I_{0J}/I_{01})(\nu_{01}/\nu_{0J})$ and A_{01} is Einstein's coefficient of spontaneous emission between the $^5D_0$ and $^7F_1$ levels, which is 50 s^{-1}. In addition, I_{0J} and ν_{0J} denote the integrated proportion and energy core of the emission band, $^5D_0-^7F_J$, respectively. Moreover, the relationship among the lifetime (τ) and radiative (A_{rad}) and nonradiative (A_{nrad}) transition rates can be defined as[54]

$$\tau = (A_{rad} + A_{nrad})^{-1} \quad (8)$$

Finally, the $^5D_0$ quantum efficiency was obtained by using the values for A_{rad} and A_{nrad} in eq 6. The lifetime and $^5D_0$ quantum efficiency are complied in Table 3. As shown in Table 3, for the

Table 3. Decay Time and Luminescence Quantum Efficiency, η (%), of Polymorphs When Reacted at Given Temperatures for 12 h

hydrothermal temperature (°C)	decay time (λ_{ex} = 394 nm) (ms)	η (λ_{ex} = 394 nm) (%)	nonradiative part (%)
100	0.63	9.33	90.67
120	0.70	10.77	89.23
140	2.00	28.76	71.24
160	2.33	33.34	66.66
180	2.47	36.09	63.91
200	2.44	35.38	64.62
220	2.27	33.14	66.86
240	1.97	29.10	70.90

sample prepared at 100 °C, the quantum efficiency is relatively low, indicating a high nonradiative part arising from the luminescence quenching of the $^5D_0$ emitting level by OH oscillators mainly from the water molecules in hydrated HP. When reacted at 120 °C, the quantum efficiency slightly increased. Strikingly, as HP transforms into LTMP when reacted at 160 °C, the quantum efficiency significantly increased up to 33.34%, about 3 times higher than that of HP. The quantum efficiency reached a maximum at 180 °C. Further, as HP appeared, the quantum efficiency showed a continuous decrease. For instance, when reacted at 200 °C, the quantum efficiency was 35.38%, which decreased to 29.10% when reacted at 240 °C. Therefore, the luminescence performance of $BiPO_4$/Eu is clearly indicated to show a strong dependence on polymorphs.

3.4. Structural Fundamentals for Polymorph-Sensitive Luminescence. The lattice prameters and atomic positions listed in Table S2 of the Supporting Information were used to build the crystal structures for both phases of $BiPO_4$. As shown in Figure 9, both structures were similarly constructed by

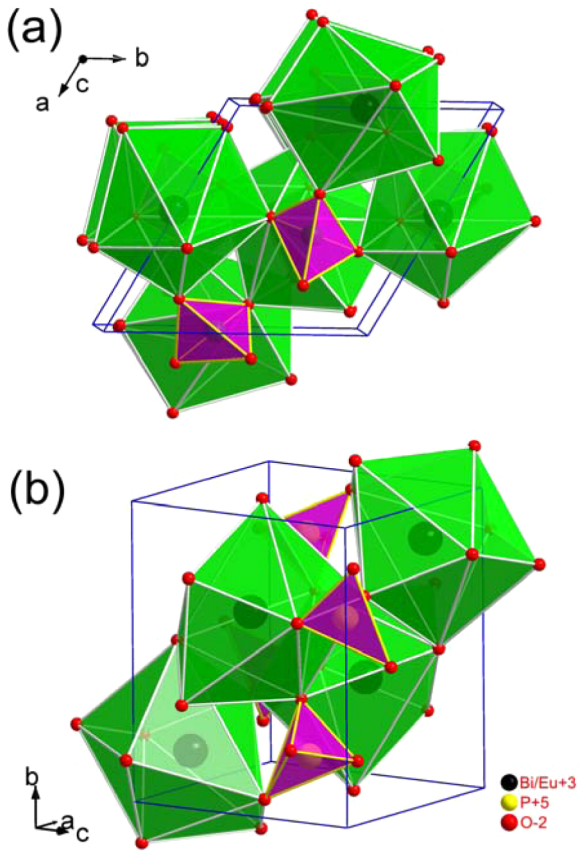

Figure 9. Crystal structures of (a) HP and (b) LTMP with Bi−O polyhedra and P−O tetrahedra. Crystal structures are drawn with the diamond program using the atomic coordinates given in Table S2.

building blocks of PO_4 and BiO_8 polyhedra, except for polyhedral arrangements and bond lengths. For HP, as indicated in Figure 9a, the structure consists of an open framework structure due to the symmetrical arrangement of chains of alternating BiO_8 polyhedra and PO_4 tetrahedra with lattice water molecules that are located in the channels parallel to the *c*-axis. Four types of Bi−O bonds are found in this structure, and the corresponding bond lengths were listed in Table S1. Comparatively, for LTMP (Figure 9b), the chains are arranged less symmetrically; hence, the structure consists of a compact space-filling network with eight different Bi−O bond lengths (Table S1).

As discussed above, in hydrothermal systems, phase formation and evolution processes were quite different from the calcination processes, which could influence the energy transfer process and electronic structure, and thus the luminescence performance. To understand the variations of luminescence properties of different polymorphs of $BiPO_4$/Eu, several structural factors, such as the local symmetry environment of Eu^{3+} ions, lattice water, and dipole moment of Bi(Eu)−O polyhedra, have to be addressed. With regard to the symmetric environment of Eu^{3+}, the symmetry for the lattice site of Eu^{3+} in both polymorphs follows such a sequence: HP > LTMP, which has been demonstrated by the variations in structural symmetry, and J−Ω parameters. Hence, the luminescence performance for $BiPO_4$/Eu is expected to decrease with the symmetric enhancement, as previously reported for $LaPO_4$/Eu of different polymorphs.[49] This expectation is in accordance with what we observed in $BiPO_4$

dx.doi.org/10.1021/cg300451d | Cryst. Growth Des. 2012, 12, 3983−3991

polymorphs. Another important factor could be from the lattice water: its impact on luminescence properties gradually becomes insignificant as HP transforms to LTMP. Especially, hydration for HP has shown a quenching effect on luminescence.

With regard to the dipole moment, considering their structural parameters, the dipole moment of polymorphs can be estimated according to the following equation,

$$\vec{\mu} = q\vec{r} \quad (9)$$

where $\vec{r}$ is the displacement vector pointing from the negative charge to the positive charge.

The values of the dipole moment in Bi(Eu)−O polyhedra are 0.181 and 1.435 D for HP and LTMP, respectively. The larger dipole moment for LTMP means that the dopant Eu^{3+} resides at sites more deviated from the centers of positive and negative charges. Meanwhile, the LTMP phase possesses stronger emission intensity and a longer decay time, which indicates that the dipole moment may be responsible for the variation trends of luminescence performance for Eu^{3+} in these polymorphs. Considering all these structural factors, the LTMP phase has shown a superior luminescence performance.

4. CONCLUSION

Eu^{3+}-doped $BiPO_4$ of different polymorphs was prepared via a hydrothermal method. With the polymorphs changes in the hydrothermal treatment process, three striking microstructure features were observed: (i) morphological change from nanorods to prismlike shape; (ii) a decrease in symmetry of tetragonal PO_4 groups from pseudo-T_d to C_1; and (iii) the variation of lattice strain from the tensile to compressive, and then to tensile. The impacts of polymorphs on luminescence properties were also clearly indicated by the changes in decay time, quantum efficiency, and nonradiative transition, in which several structural factors, such as the symmetric environment of Eu^{3+}, lattice water, and the dipole moment of Bi(Eu)−O polyhedra contribute to the polymorph-sensitive luminescence properties, leading to a superior luminescence for LTMP. The results reported in this work may pave a novel way to tailor the luminescence properties for many applications through systematic control over the polymorphs in hydrothermal systems.

■ ASSOCIATED CONTENT

Supporting Information

Rietveld refinements on the raw data; XRD patterns of the samples prepared at given conditions; rector for the sample preparation; lattice parameters, atomic positions, and bond lengths of $BiPO_4$ polymorphs. This material is available free of charge via the Internet at http://pubs.acs.org.

■ AUTHOR INFORMATION

Corresponding Author

*E-mail: lipingli@fjirsm.ac.cn.

Notes

The authors declare no competing financial interests.

The authors declare no competing financial interest.

■ ACKNOWLEDGMENTS

This work was financially supported by NSFC (No. 21025104, 51072198, 50972143) and the National Basic Research Program of China (No. 2011CBA00501). The authors express their thanks to Dr. Peng Wang from Fuzhou University for photoluminescence measurements.

■ REFERENCES

(1) Feng, S. H.; Xu, R. R. *Acc. Chem. Res.* **2001**, *34*, 239−247.
(2) Zhu, Y.; Mei, T.; Wang, Y.; Qian, Y. *J. Mater. Chem.* **2011**, *21*, 11457−11463.
(3) Sardar, K.; Lees, M. R.; Kashtiban, R. J.; Sloan, J.; Walton, R. I. *Chem. Mater.* **2011**, *23*, 48−56.
(4) Marques, V. S.; Cavalcante, L. S.; Sczancoski, J. C.; Alcântara, A. F. P.; Orlandi, M. O.; Moraes, E.; Longo, E.; Varela, J. A.; Siu, Li, M.; Santos, M. R. M. C. *Cryst. Growth Des.* **2010**, *10*, 4752−4768.
(5) Huang, X. H.; Tay, C. B.; Zhan, Z. Y.; Zhang, C.; Zheng, L. X.; Venkatesan, T.; Chua, S. J. *CrystEngComm* **2011**, *13*, 7032−7036.
(6) Jannasch, H. W.; Mottl, M. J. *Science* **1985**, *229*, 717−725.
(7) Thornton, T. D.; Savage, P. E. *Ind. Eng. Chem. Res.* **1992**, *31*, 2451−2456.
(8) Demazeau, G. *J. Mater. Sci.* **2008**, *43*, 2104−2114.
(9) Raoux, S.; Welnic, W.; Ielmini, D. *Chem. Rev.* **2010**, *110*, 240−267.
(10) Liu, J. F.; Li, Q. H.; Wang, T. H.; Yu, D. P.; Li, Y. D. *Angew. Chem., Int. Ed.* **2004**, *43*, 5048−5052.
(11) Jia, C. J.; Sun, L. D.; You, L. P.; Jiang, X. C.; Luo, F.; Pang, Y. C.; Yan, C. H. *J. Phys. Chem. B* **2005**, *109*, 3284−3290.
(12) Ghosh, P.; Patra, A. *J. Phys. Chem. C* **2008**, *112*, 19283−19292.
(13) Lai, H.; Bao, A.; Yang, Y.; Tao, Y.; Yang, H. *CrystEngComm* **2009**, *11*, 1109−1113.
(14) Wang, F.; Han, Y.; Lim, C. S.; Lu, Y.; Wang, J.; Xu, J.; Chen, H.; Zhang, C.; Hong, M.; Liu, X. *Nature* **2010**, *463*, 1061−1065.
(15) Yang, J.; Li, C.; Zhang, X.; Quan, Z.; Zhang, C.; Li, H.; Lin, J. *Chem.—Eur. J.* **2008**, *14*, 4336−4345.
(16) Jia, C.-J.; Sun, L.-D.; Luo, F.; Jiang, X.-C.; Wei, L.-H.; Yan, C.-H. *Appl. Phys. Lett.* **2004**, *84*, 5305−5307.
(17) Kudo, A.; Omori, K.; Kato, H. *J. Am. Chem. Soc.* **1999**, *121*, 11459−11467.
(18) Wang, X.; Loa, I.; Syassen, K.; Hanfland, M.; Ferrand, B. *Phys. Rev. B* **2004**, *70*, 064109.
(19) Zhao, M.; Li, G.; Zheng, J.; Li, L.; Wang, H.; Yang, L. *CrystEngComm* **2011**, *13*, 6251−6257.
(20) Guan, M. Y.; Sun, J. H.; Tao, F. F.; Xu, Z. *Cryst. Growth Des.* **2008**, *8*, 2694−2697.
(21) Toby, B. H. *J. Appl. Crystallogr.* **2001**, *34*, 210−213.
(22) Mooney-Slater, R. C. L. *Z. Kristallogr.* **1962**, *117*, 371−385.
(23) Pitcher, M. W.; Ushakov, S. V.; Navrotsky, A.; Woodfield, B. F.; Li, G. S.; Boerio-Goates, J.; Tissue, B. M. *J. Am. Ceram. Soc.* **2005**, *88*, 160−167.
(24) Yagi, T.; Utsumi, W.; Yamakata, M.-a.; Kikegawa, T.; Shimomura, O. *Phys. Rev. B* **1992**, *46*, 6031−6039.
(25) Li, G. S.; Li, L. P.; Boerio-Goates, J.; Woodfield, B. F. *J. Am. Chem. Soc.* **2005**, *127*, 8659−8666.
(26) Romero, B.; Bruque, S.; Aranda, M. A. G.; Iglesias, J. E. *Inorg. Chem.* **1994**, *33*, 1869−1874.
(27) Poloznikova, M. E.; Fomichev, V. V. *Usp. Khim.* **1994**, *63*, 419−430.
(28) Pawlig, O.; Schellenschlager, V.; Lutz, H. D.; Trettin, R. *Spectrochim. Acta: Part a: Mol. Biomol. Spectrosc.* **2001**, *57*, 581−590.
(29) Assaaoudi, H.; Ennaciri, A.; Rulmont, A. *Vib. Spectrosc.* **2001**, *25*, 81−90.
(30) Silva, E. N.; Ayala, A. P.; Guedes, I.; Paschoal, C. W. A.; Moreira, R. L.; Loong, C. K.; Boatner, L. A. *Opt. Mater.* **2006**, *29*, 224−230.
(31) Nakamoto, K. *Infrared and Raman Spectra of Inorganic and Coordination Compounds, part A*; John Wiley and Sons: New York, 1986.
(32) Kravitz, L. C.; Kingsley, J. D.; Elkin, E. L. *J. Chem. Phys.* **1968**, *49*, 4600−4610.
(33) Xue, F.; Li, H. B.; Zhu, Y. C.; Xiong, S. L.; Zhang, X. W.; Wang, T. T.; Liang, X.; Qian, Y. T. *J. Solid State Chem.* **2009**, *182*, 1396−1400.
(34) Begun, G. M.; Beall, G. W.; Boatner, L. A.; Gregor, W. J. *J. Raman Spectrosc.* **1981**, *11*, 273−278.
(35) Geng, J.; Hou, W. H.; Lv, Y. N.; Zhu, J. J.; Chen, H. Y. *Inorg. Chem.* **2005**, *44*, 8503−8509.

(36) Li, G. S.; Boerio-Goates, J.; Woodfield, B. F.; Li, L. P. *Appl. Phys. Lett.* **2004**, *85*, 2059−2061.
(37) Williamson, G. K.; Hall, W. H. *Acta Metall.* **1953**, *1*, 22−31.
(38) Li, L. P.; Su, Y. G.; Li, G. S. *J. Mater. Chem.* **2010**, *20*, 459−465.
(39) Naidu, B. S.; Vishwanadh, B.; Sudarsan, V.; Vatsa, R. K. *Dalton Trans.* **2012**, *41*, 3194−3203.
(40) Wolfert, A.; Oomen, E. W. J. L.; Blasse, G. *J. Solid State Chem.* **1985**, *59*, 280−290.
(41) Zhu, H.; Li, R.; Luo, W.; Chen, X. *Phys. Chem. Chem. Phys.* **2011**, *13*, 4411−4419.
(42) Zhao, M.; Li, G.; Zheng, J.; Li, L.; Yang, L. *CrystEngComm* **2012**, *14*, 2062−2070.
(43) Werts, M. H. V.; Jukes, R. T. F.; Verhoeven, J. W. *Phys. Chem. Chem. Phys.* **2002**, *4*, 1542−1548.
(44) Huang, J.; Loriers, J.; Porcher, P. *C. R. Acad. Sci. Ser. II* **1982**, *294*, 545−548.
(45) Malta, O. L.; Brito, H. F.; Menezes, J. F. S.; Silva, F.; Alves, S.; Farias, F. S.; deAndrade, A. V. M *J. Lumin.* **1997**, *75*, 255−268.
(46) Boyer, J. C.; Vetrone, F.; Capobianco, J. A.; Speghini, A.; Bettinelli, M. *J. Phys. Chem. B* **2004**, *108*, 20137−20143.
(47) Ofelt, G. S. *J. Chem. Phys.* **1962**, *37*, 511−520.
(48) Judd, B. R. *Phys. Rev.* **1962**, *127*, 750−761.
(49) Ghosh, P.; Kar, A.; Patra, A. *J. Appl. Phys.* **2010**, *108*, 113506.
(50) Carnall, W. T. C. H.; Crosswhite, H. M. *Energy level structure and transition probabilities in the spectra of the trivalent lanthanides in* LaF_3; Argonne National Laboratory: Argone, IL, 1978.
(51) Peng, C. Y.; Zhang, H. J.; Yu, J. B.; Meng, Q. G.; Fu, L. S.; Li, H. R.; Sun, L. N.; Guo, X. M. *J. Phys. Chem. B* **2005**, *109*, 15278−15287.
(52) Su, Y. G.; Li, L. P.; Li, G. S. *Chem. Mater.* **2008**, *20*, 6060−6067.
(53) Li, L. P.; Zhao, M. L.; Tong, W. M.; Guan, X. F.; Li, G. S.; Yang, L. S. *Nanotechnology* **2010**, *21*, 195601.
(54) Lorbeer, C.; Cybinska, J.; Mudring, A.-V. *Cryst. Growth Des.* **2011**, *11*, 1040−1048.